

# PROCEEDINGS OF SPIE

[SPIDigitalLibrary.org/conference-proceedings-of-spie](https://spiedigitallibrary.org/conference-proceedings-of-spie)

## Soft x-ray linear dichroic ptychography: the study of crystal orientation in biominerals

Vanessa Schoeppler, Matthew Marcus, Young-Sang Yu,  
Richard Celestre, Karen Bustillo, et al.

Vanessa Schoeppler, Matthew A. Marcus, Young-Sang Yu, Richard S. Celestre, Karen C. Bustillo, Roger Falcone, David A. Shapiro, "Soft x-ray linear dichroic ptychography: the study of crystal orientation in biominerals," Proc. SPIE 11839, X-Ray Nanoimaging: Instruments and Methods V, 118390D (8 September 2021); doi: 10.1117/12.2594172

**SPIE.**

Event: SPIE Optical Engineering + Applications, 2021, San Diego, California, United States

# Soft x-ray linear dichroic ptychography: The study of crystal orientation in biominerals

Vanessa Schoeppler<sup>\*a</sup>, Matthew A. Marcus<sup>b</sup>, Young-Sang Yu<sup>b</sup>, Richard S. Celestre<sup>b</sup>, Karen C. Bustillo<sup>c</sup>, Roger Falcone<sup>a</sup>, David A. Shapiro<sup>b</sup>

<sup>a</sup> Department of Physics, University of California, Berkeley, USA; <sup>b</sup> Advanced Light Source, Lawrence Berkeley National Laboratory, Berkeley, USA; <sup>c</sup> National Center for Electron Microscopy, Molecular Foundry, Lawrence Berkeley National Laboratory, Berkeley, CA, USA

## ABSTRACT

Here we present soft X-ray linear dichroic ptychography developed at the COherent Scattering and MICROscopy (COSMIC) beamline at the Advanced Light Source (ALS) by studying biominerals—complex 3D hierarchically structured mineral-organic composite materials—produced by living organisms. Sequences of soft x-ray ptychography images at varying EPU polarizations were acquired, which principally allows visualization and orientation mapping of complex biogenic ultrastructures with spatial resolution down to 8 nm. These correlative data not only shed light on key mechanisms of the formation and mechanical principles of these composites but also demonstrate the capabilities and limitations of this newly developed technique, such as orientational precision, angular resolution and thickness related restrictions.

**Keywords:** ptychography, linear dichroism, biomineralization, soft x-rays

\*vschoeppler@lbl.gov

## 1. INTRODUCTION

Chemical-specific x-ray linear dichroism is a powerful technique that provides orientational information of optically anisotropic materials, such as certain biomolecules, polymers, fibers and composites, by measuring local changes of the material's complex refractive index as a function of incident beam polarization and energy<sup>1,2</sup>. This linear polarization-dependent imaging contrast (PIC) has routinely been used to quantify crystal orientation in biominerals using x-ray photoemission electron microscopy in reflection geometry achieving a spatial resolution of several tens of nanometers<sup>3</sup>. Yet, biominerals—produced by living organisms—are complex 3D hierarchically structured mineral-organic composite materials that can be composed of mineral units as small as a few nanometers. While the complex architecture is known to affect the physical properties of the minerals that are drastically improved compared to the pure mineral<sup>4</sup>, it also complicates comprehensive analysis of the material. Correlative analysis of structure, composition and crystal orientation from macro to nanoscale is essential and has been key to recent formulations of physical and kinetic models that explain the evolution of crystal morphologies in biominerals<sup>5,6</sup>. However, high-resolution orientational analysis of biominerals remains a challenging task, since many established techniques provide limited spatial resolution (e.g. EBSD, 3DXRD, PEEM-PIC mapping) or allow investigation of small areas only (e.g. electron nanodiffraction, Bragg ptychography). Recently, linear dichroic ptychography has been successfully used by utilizing hard and soft x-rays<sup>7,8</sup>. The latter was used at the COSMIC beamline at the ALS<sup>8</sup>, allowing high resolution imaging (down to 8 nm) of comparatively large areas (several square micrometers)<sup>9</sup>. They mapped the c-axis orientation in calcium carbonate based multi crystalline coral fragments by analyzing four different polarization angles only, because, initially, the sample had to be rotated manually, since the EPU control was only calibrated for linear horizontal and vertical polarizations. Now an automatic EPU control has been implemented, which allows free adjustment of the polarization angles between 0° and 90°. In addition, data acquisition and reconstruction has been automated. To determine the orientational precision, angular resolution and thickness related limitations of the system, a geological aragonite standard sample and a biogenic calcite sample were prepared using a focused ion beam (FIB) scanning electron microscope (SEM) and investigated with scanning transmission x-ray microscopy (STXM) and Ptychography, respectively.

## 2. MEASUREMENTS AND RESULTS

### 2.1 Linear dichroic STXM analysis of an aragonite standard

A rectangular lift-out sample, with the long axis parallel to the aragonite c-axis (Fig. 1a), was prepared from a geological aragonite crystal at the National Center for Electron Microscopy (NCEM), Molecular Foundry, Lawrence Berkeley National Laboratory, Berkeley, CA (USA), using a FEI Helios G4 UX dual beam Focused Ion Beam, utilizing a focused Ga<sup>+</sup> ion beam for site-selective material removal and a field emission scanning electron microscope (SEM) column for imaging, following a standard u-cut FIB lift-out procedure. After lift-out the sample was welded to an Omniprobe 3 Post Cu Lift-out Grid and thinned to a triangular shape with increasing thickness from left to right (Fig. 1b). The TEM investigations and corresponding diffraction patterns of the sample (Fig. 1c) were also performed at NCEM, utilizing a FEI TitanX 60-300 microscope operating at 300 kV accelerating voltage. The diffraction pattern was acquired from an illuminated area of ~4 μm in diameter to cover the main part of the sample and indexed with the Crystallographic Tool Box (CrysTBox)<sup>10</sup>, which confirmed that the aragonite c-axis is parallel to the long axis of the sample (red arrow).

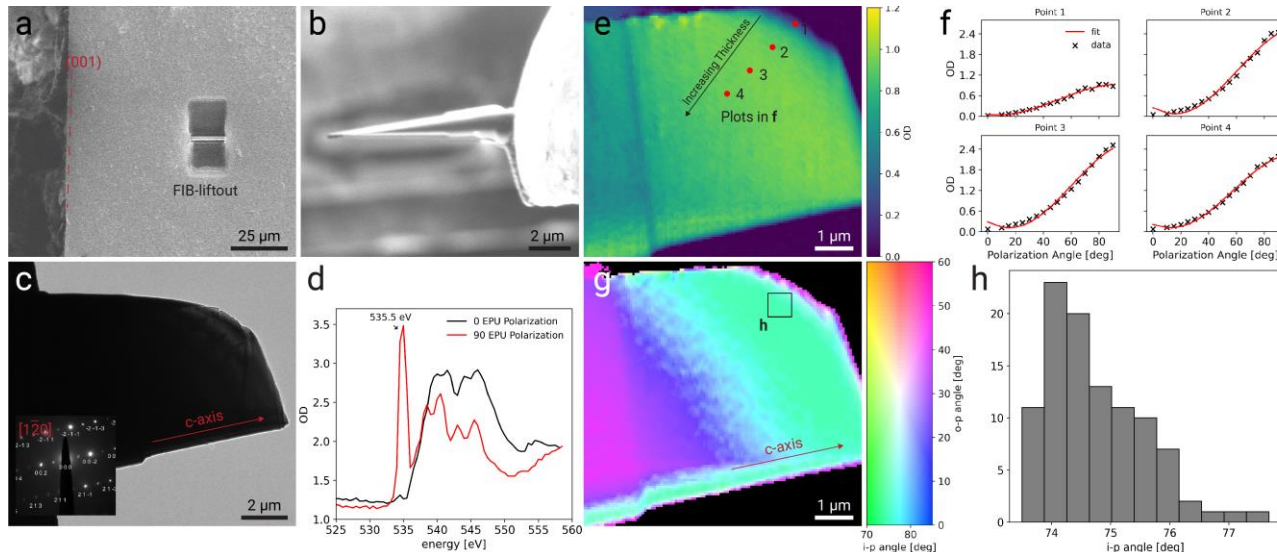


**Figure 1. TEM and STXM orientational analysis of an aragonite standard.** **a)** SEM image of the extraction site of the FIB lift-out sample. FIB lamella was prepared with its long axis perpendicular to the aragonite (001) plane. **b)** Top view of the lamella welded to a TEM grid and thinned to a triangular shape with increasing thickness from left to right. **c)** TEM image of the sample (side view); the c-axis is indicated as red arrow and was determined by the corresponding large area diffraction pattern (inset). **d)** Oxygen K-edge NEXAFS spectra of the aragonite sample obtained in STXM mode and at 2 different EPU-polarizations. **e-h)** Analysis of a STXM stack of the aragonite sample acquired at 535.5 eV (on-peak) and at 19 polarization angles, varying from horizontal (EPU polarization angle = 90 °) to vertical (EPU polarization angle = 0 °). **e)** Mean intensity projection of the stack with the pre-edge image acquired at 530 eV subtracted. **f)** Plots of the pixel intensity data extracted at the points indicated in **e)**. **g)** Polarization-dependent Imaging Contrast (PIC) maps of the aragonite sample; the color key on the right indicates the crystal in- and out-of-plane c-axis angle (determined from the Malus law fit in **f)** corresponding to the azimuth and amplitude, respectively; the calculated average in-plane c-axis angle from the area marked with a black box is indicated with a red arrow; the relative 0 deg axis is vertical in the image. **h)** Histogram of the in-plane c-axis angle distribution from the area indicated in **g)** covering 10x10 pixels.

To investigate the aragonite sample at the COSMIC beamline with PIC, first oxygen K-edge line spectra at 0° and 90° EPU polarization were acquired, by varying the energy from 500 to 560 eV with a 0.5 eV step and a total of 5x10<sup>5</sup>

photons per pixel. The transmitted intensity was collected with a silicon photodiode with an active area of 2 mm by 5 mm, for each polarization. Coherent and monochromatic x-rays were focused onto the sample using a Fresnel zone plate, with 45-nm outer zone width. The corresponding spectra are shown in Figure 1d. It demonstrates that the maximum of the typical O K-edge  $\pi^*$  peak, the absorption of which is strongly dependent on the polarization<sup>8</sup>, is at 535.5 eV. A series of conventional STXM images using the same basic setup were acquired “on-peak” at 535.5 eV, with a 60 nm step size and at 19 polarization angles, varying from horizontal (EPU polarization angle = 90 °) to vertical (EPU polarization angle = 0 °). One pre-edge image was acquired at 530.0 eV where the transmitted intensity should not depend on the polarization and was subtracted from the entire image stack after alignment to correct for thickness related changes in absorption. The corrected average intensity projection of the calculated optical density (OD), which is the  $\ln(I_0/I)$ , of the image stack is shown in Figure 1e. Variations in optical density should not be associated with differences in crystal orientation since the investigated sample is a single crystal. Thus, despite pre-edge subtraction the thickness still affects the intensity which is used to determine the c-axis angle. In Figure 1f the plots of the pixel optical density data extracted at the points indicated in Figure 1e, which follow the thickness gradient of the sample. Typical for PIC mapping<sup>3</sup> the data were fitted to the Malus law:  $f(\text{EPU}^\circ) = \alpha + \beta \cos^2(\text{EPU}^\circ - c')$ . In the Malus law the fit parameter  $c'$  represents the in-plane angle of the crystal's c-axis, which corresponds to the azimuth of the cosine, and  $\beta/\alpha$  is related to the off-plane angle, which is affected by the amplitude of the curve. The polarization dependence is clearly visible and despite increasing thickness the data were fitted nicely for each pixel. In addition, the maximum OD for points 2 to 4 stays constant assuming that the pre-edge subtraction successfully corrected for thickness variations for ODs up to 2.4 for aragonite. Figure 1g displays the final PIC map where each pixel has been fitted using a Python code that was based on the original GG Macro developed by P. Gilbert's group<sup>3</sup>. In the PIC map the thickness effect is more obvious, whereas the off-plane c-axis angle is more affected as it is correlated to the amplitude. The homogeneous cyan region marks a region with appropriate thickness to map the crystal orientation. The red arrow represents the in-plane c-axis angle of aragonite, which was calculated as the mean value of all pixels marked by the black box and differs by only half a degree from the in-plane c-axis angle determined by TEM (Fig. 1c). Yet, the angular spread demonstrated by the histogram in Figure 1h is with approximately 3 degrees, quite high due to the noise in STXM images.

## 2.2 Analysis of crossed-foliated calcite with x-ray linear dichroic ptychography

Similar to crossed lamellar aragonite—the most abundant molluscan shell ultrastructure<sup>11</sup>—crossed foliated calcite found in the shell of the gastropod *Patella vulgata*, is known for its complex hierarchical organization into several different orders of lamellae. The largest structural units are the 1<sup>st</sup> order lamellae that are typically several tens of micrometer thick and show alternating crystallographic orientation every other lamella. The 1<sup>st</sup> order lamellae themselves are composed of approximately 200 nm thick sheet-like arrangement, the 2<sup>nd</sup> order lamellae, which again are composed of individual calcite rods, termed 3<sup>rd</sup> order lamellae<sup>12</sup>. Despite this lamellar architecture being the most common structural arrangement in molluscan shells, there is currently no clear explanation for its formation, in contrast to the well-studied nacreous and prismatic architectures, whose morphogenesis could recently be described with physical models<sup>6,13</sup>. The development of these models heavily depended on the ability to fully analyze the morphological and crystallographic properties of the relatively coarse mineral building units. However, the delicate fibrous mineral units in foliated and lamellar architectures are only a few tens of nanometer thick and are highly sensitivity to beam damage, which makes it one of the most challenging ultrastructures to study and a great candidate for x-ray linear dichroic ptychography.

Figure 2a displays the diamond polished surface of a transversal cross-section of a *Patella vulgata* shell, showing the typical two-layered shell arrangement with an aragonitic layer at the top and the crossed foliated calcite layer at the bottom. The 1<sup>st</sup> order lamellae are clearly distinguishable by their difference in contrast and run roughly perpendicular to the outer shell layer. The same experimental setup as described above for the aragonite sample was used to prepare a FIB lift-out sample, which has been extracted parallel to the long axis of a 1<sup>st</sup> order lamella and thinned to a uniform rectangular shape with a final thickness of 100 to 200 nm (Figs. 2b and 1c). The STEM image in Figure 2 was also acquired at NCEM using a FEI TitanX 60-300 microscope operating at 300 kV accelerating voltage and shows the individual 2<sup>nd</sup> order layer as thinner than expected 50 to 100 nm thick layers. The difference in contrast indicates misorientation between the layers, which was analyzed with linear dichroic ptychography at COSMIC.

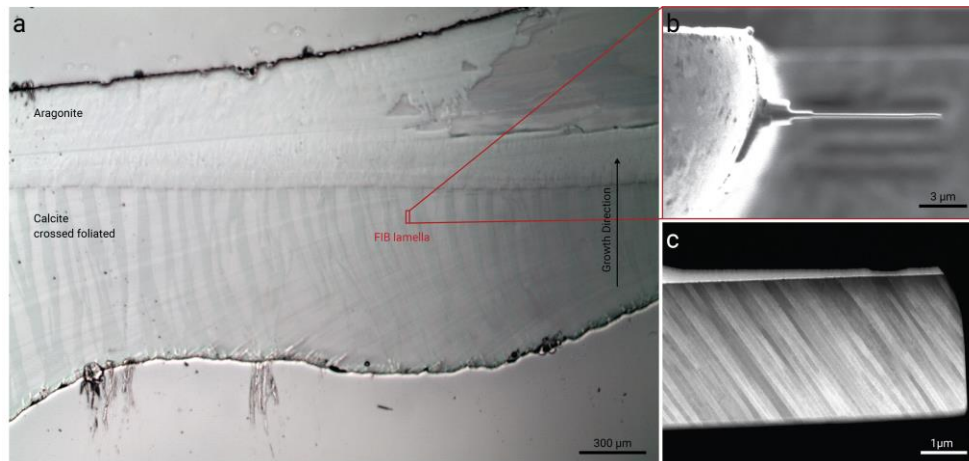


**Figure 2. Crossed foliated calcite sample from a limpet shell.** a) Optical light microscopy image of a polished cross-section of a *Patella vulgata* shell prepared perpendicular to the shell's outer surface, showing its two main calcite and aragonite layers and the first order lamella composing the crossed foliated calcite layer (bottom half) b) Top view of the FIB lift-out sample extracted from the region indicated in a with its long axis normal to the shell surface. c) STEM image of the thinned lift-out sample, showing the 2<sup>nd</sup> order lamella.

Similar to the aragonite standard, the energy of the O K-edge  $\pi^*$  peak maximum of the crossed foliated calcite sample was determined with a NEXAFS line scan as 535.5 eV (not shown). To reduce beam absorption and attenuation caused by specimen thickness the “on-peak” energy was chosen to be slightly off the maximum absorption peak at 535.0 eV. Ptychographic measurements consisted of single diffraction patterns recorded with a fast frame rate charge coupled device (CCD) at each scan point with 100/10 ms double exposure dwell time and scanned with 60-nm steps, 25  $\mu\text{m}$  out of focus, covering an area of 4 x 6  $\mu\text{m}$  and 14 polarization angles, varying from horizontal (EPU polarization angle = 90°) to vertical (EPU polarization angle = 0°). A pre-edge image was recorded under the same conditions at 530 eV and 0° polarization. Ptychography reconstructions were performed by using an alternating projection algorithm<sup>14</sup> with 1000 iterations (including probe and background refinement) and the reconstruction pixel size was reduced to 20 nm/pixel to reduce noise.

Figure 3a shows an exemplary OD image of the polarization stack with the pre-edge image subtracted. Individual lamellae are discernible and a gradient in thickness is visible as well, which is a typical artifact from the FIB thinning process. However, its effect was not eliminated completely by pre-edge subtraction. The polarization plots in Figures 3b-3c confirm an increase in thickness as the maximum OD increases from 1 to 3 from left to right. Interestingly, the polarization dependency of the  $\pi^*$  peak intensity is strongly affected by the thickness, resulting in skewed data shape that does not reflect a perfect cosine shape (Figs. 3b-3d). This is different to aragonite (Fig. 1f) where at an OD of 3 the data still resembled a perfect cosine curve and resulted in a sufficient fit result. In calcite, however, thicker regions result in inaccurate fit results for both amplitude and azimuth affecting the calculated in- and out-of-plane angle, visible in the final PIC map (Fig. 4a). The difference in absorption remains puzzling to us, as in both cases the  $\pi^*$  orbitals of the planar carbonate group govern the dichroism, which have their dipole moments along the long c-axis (i.e. 17.06 Å) of the trigonal crystal system in calcite and the shorter c-axis of the orthorhombic crystal system in aragonite (i.e. 5.74 Å). Both crystals are built of alternating layers of calcium atoms and the planar carbonate groups, whereas 3 unit cells of aragonite match the number of planes of 1 calcite unit cell, and thus, should show similar strong dichroism. The highest OD regions of the calcite sample (lowest transmission) also show ptychographic reconstruction artefacts, which show oscillations characteristic of the probe structure. Improper probe refinement due to low transmission could reduce the overall resolution of the images. Similar artifacts are not expected to occur in the aragonite sample as the specimen was investigated in STXM mode.

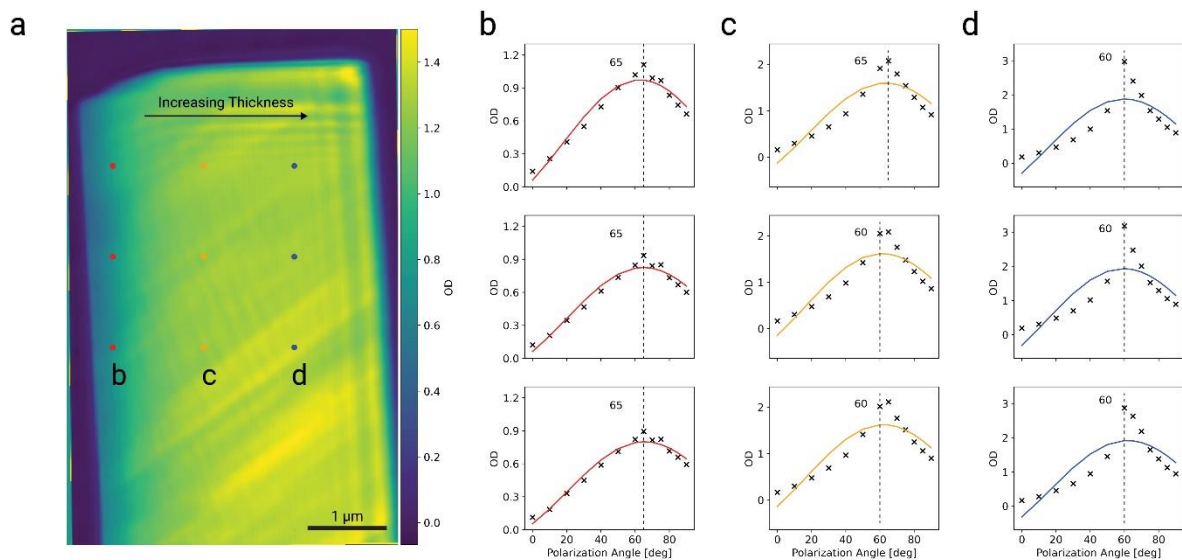


**Figure 3. High resolution orientational analysis of the calcite lamella using x-ray linear dichroic ptychography. a)** Exemplary optical density image of a ptychography image stack acquired with a photon energy of 535 eV (0.5 degree off-peak to reduce thickness related absorption issues) and at 14 polarization angles, varying from horizontal (EPU polarization angle =  $90^\circ$ ) to vertical (EPU polarization angle =  $0^\circ$ ). A pre-edge image was acquired at 530 eV and  $0^\circ$  polarization angle and subtracted from the entire stack. **b-d)** Plots of the pixel intensity data extracted at the points indicated in **a**, with the thickness increasing form left to right.

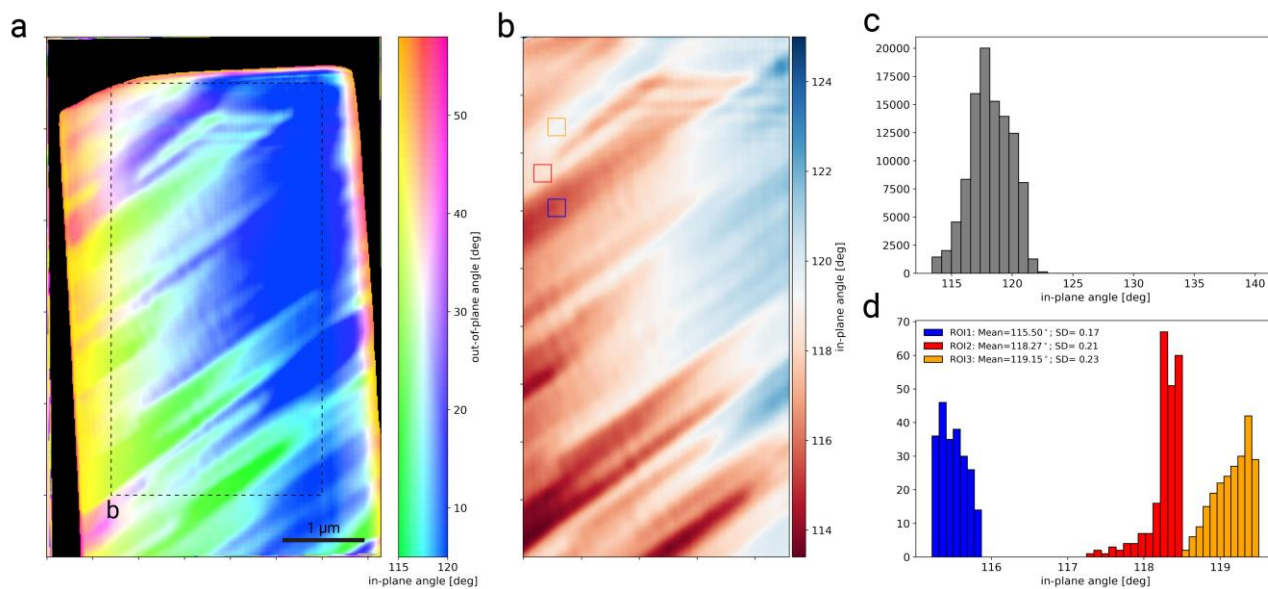


**Figure 4: X-ray linear dichroic ptychography analysis of foliated calcite. a)** PIC map of the calcite lift-out sample; the color key on the right indicates the crystal c-axis with the azimuth and amplitude corresponding to the in- and out-of-plane c-axis angle, respectively; the relative 0 deg axis is horizontal in the image. **b)** Map of the in-plane c-axis angle (azimuth) of the region indicated in **a**, avoiding the edge artefacts. **c)** Histogram of the in-plane c-axis angle of the entire area mapped in **b**. **d)** Histograms, average angular distributions and standard deviations of the ROIs indicated as squared boxes in **b**, corresponding to individual 2<sup>nd</sup> order lamella and covering 15x15 pixels, respectively.

The image shows gradient from left to right representing the out-of-plane angle (Fig. 4a). This gradient is false as the 1<sup>st</sup> order lamellae are known to have a consistent crystal orientation over several tens of micrometers. Yet, the relative changes in the in-plane angle along the vertical image direction are valid. In Figure 4b only the in-plane angle of the region indicated in Figure 4a is mapped ignoring the edge artefacts and showing that the c-axis angle of the 2<sup>nd</sup> order lamellae tilts back and forth by a few degrees. The histogram in Figure 4c represents the in-plane c-axis angle of the entire region mapped in Figure 4b and shows angular distribution of about 5 degrees. However, comparing the regions marked in Figure 4b shows that the individual orientations of the lamellae can clearly be distinguished and differ by 1 to 2 degrees. The calculated standard deviations within the regions indicate an angular resolution that lies below a degree. Ptychographic PIC measurements on single crystalline standards are planned to confirm the comparatively high angular resolution.

### 3. CONCLUSIONS

We demonstrated that the automatic EPU and data acquisition control, as well as the adjusted data analysis algorithms, implemented at COSMIC, can successfully be used to generate and analyze linear dichroic STXM and ptychography data. This allows high resolution complementary analysis of structure, composition and crystal orientation of complex dichroic materials, such as biominerals, by utilizing various capabilities of the endstation. The data presented here indicate a high angular precision compared to TEM data and an angular resolution better than a degree. We further showed that, in order to obtain high quality orientation information, the thickness of the test specimen has to be controlled, whereas the thickness threshold has to be determined for different materials individually. Nevertheless, we showed that high-resolution linear dichroic analysis of complex materials such as crossed-foliated calcite can be used to reveal rarely accessible crystallographic and structural details, which are essential to decipher the formation process and physical properties of the material. This will help to deepen our understanding of evolution-driven materials design and provide biomimetic inspiration.

### ACKNOWLEDGEMENTS

V.S. acknowledges support from STROBE: A National Science Foundation Science & Technology Center, under Grant No. DMR-1548924. This research used resources of the Advanced Light Source, a U.S. DOE Office of Science User Facility under contract no. DE-AC02-05CH11231. Work at the Molecular Foundry was supported by the Office of Science, Office of Basic Energy Sciences, of the U.S. Department of Energy under Contract No. DE-AC02-05CH11231.

### REFERENCES

- [1] Nordén, B., "Applications of linear Dichroism Spectroscopy," *Appl. Spectrosc. Rev* 14(2),157-248 (1978)
- [2] Ade, A., Hsiao, B., "X-ray Linear Dichroism Microscopy," *Science* 262(5138), 1427-1429 (1993)
- [3] Gilbert, P., "Polarization-dependent Imaging Contrast (PIC) Mapping in 2018," *Microscopy and Microanalysis* 24(S2), 454-457 (2018).
- [4] Mann, S., [Biomineralization: Principles and Concepts in Bioinorganic Materials Chemistry], Oxford University Press, New York (2001).
- [5] Schoeppler, V., Gránásy, L., Reich, E., et al., "Biomineralization as a Paradigm of Directional Solidification: A Physical Model for Molluscan Shell Ultrastructural Morphogenesis," *Adv. Mater.* 30, 1803855 (2018)
- [6] Schoeppler, V., Lemanis, R., Reich, E., et al., "Crystal growth kinetics as an architectural constraint on the evolution of molluscan shells," *PNAS* 116(41), 20388-20397 (2019)
- [7] Gao, Z., Holler, M., Odstrcil, M., et al., "Nanoscale crystal grain characterization via linear polarization X-ray ptychography," *Chem. Commun.* 56, 13373-13376 (2020)
- [8] Lo, Y.H., Zhou, J., Rana, A., et.al, "X-ray linear dichroic ptychography," *PNAS* 118(3), e2019068118 (2021)
- [9] Shapiro A.S, Babin, S., Celestre, R.S., et. al., "An ultrahigh-resolution soft x-ray microscope for quantitative analysis of chemically heterogeneous nanomaterials," *Science Advances* 6(51), eabc4904 (2020)
- [10] Klinger, M., "More features, more tools, more CrysTBox," *J. Appl. Crystallogr* 50, 1226-1234 (2017)

- [11] Chateigner, D., Hedegaard, C., Wenk, H.R., "Mollusc shell microstructures and crystallographic textures," *Journal of Structural Geology* 22, 1723-1735 (2000)
- [12] Nouet, J., Chevallard, C., Farre, B., et al., "Limpet Shells from the Aterian Level 8 of El Harhoura 2 Cave (Témara, Morocco): Preservation State of Crossed-Foliated Layers," *PLoS ONE* 10(9): e0137162 (2015)
- [13] Beliaev, M., Zöllner, D., Pacureanu, A., et al., "Dynamics of topological defects and structural synchronization in a forming periodic tissue," *Nature Physics* 17,410-415 (2021)
- [14] Marchesini, S., Krishnan, S., Daurer B.J., et al., "SHARP: A distributed GPU-based ptychographic solver," *J. Appl. Cryst.* 49, 1245–1252 (2016)